Dalton Transactions

An international journal of inorganic chemistry

Accepted Manuscript

This article can be cited before page numbers have been issued, to do this please use: A. Zadoia, A. M. Arevalo-Lopez, J. Sanchez-Benitez, M. Huve, J. Blach, S. Merkel, N. Hilairet, J. Chantel and M. Colmont, *Dalton Trans.*, 2020, DOI: 10.1039/D0DT02721A.

ROYAL SOCIETY OF CHEMISTRY

rsc.li/dalton

View Article Online
DOI: 10.1039/D0DT02721A

ARTICLE

High pressure exploration in the Li – Ln – V – O system

Zadoya, A. I.;[a] Arévalo-López, Á. M.;[a] Sánchez-Benítez, J.;[c] Huvé,[a] M.; Blach, J.-F.;[a] Merkel, S.;[c] Hilairet, N.;[c] Chantel, J.;[c] Colmont, M. [a†]

Received 00th January 20xx,
Accepted 00th January 20xx

DOI: 10.1039/x0xx00000x

[a.]

Using *in situ* high pressure Raman spectroscopy, two structural changes were observed in a sample of composition $LiLa_5O_5(VO_4)_2$. Taking this account and by combining different conditions, three new compounds have been further obtained from high pressure – high temperature synthesis. Their crystal structure description is done using the antiphase approach, that implies the presence of oxygen-centered [O*Ln*$_4$] building units, where *Ln* is La for (1) β-$LiLa_5O_5(VO_4)_2$ and (2) β-$LiLa_2O_2(VO_4)$ or Nd for (3) $LiNd_5O_5(VO_4)_2$ compounds. (1) crystallizes in the triclinic space group *P*-1 with unit cell parameters of *a* = 5.8167(15) Å, *b* =12.2954(28) Å, *c* =18.7221(69) Å, *α* =102.03(2)°, *β* = 98.76(2)°, *γ* = 103.54(2)° and a 3D structure deduced from the ambient pressure polymorph. (2) crystallizes as well in *P*-1 with *a* = 5.8144(7) Å, *b* = 5.8167(7) Å, *c* = 8.5272(1)Å, *α* = 98.184(7)°, *β* = 100.662(7)° and *γ* = 92.579(7)°. It shows a 2D structure with $[La_2O_2]^{2+}$ layers surrounded by $[LiO_4]$ and $[VO_4]$ tetrahedra sharing corners and edges. (3) exhibits a 3D architecture isotypic with AP-$LiLa_5O_5(VO_4)_2$. The crucial role of High Pressure in such type of synthesis and materials is also discussed.

Introduction

During the last decades, many efforts have been devoted to the synthesis and characterization of new functional materials. Most of this research is focused on exploring the partial or total substitution of elements into a material, with the idea of modifying the properties. Another strong direction for that is the use of exploratory synthesis process. Apart from the traditional solid state route, hydrothermal, solvothermal or sol-gel methods, high pressure – high temperature (HP-HT) synthesis drastically modifies the thermodynamical working conditions by increasing the reactivity between precursors. It was largely used to prepare new structures containing both anions and cations in unusual coordination geometries. Since the 1970's many works are referenced. [1,2,3] Another key point is the possibility to stabilize phases that cannot be obtained at ambient conditions or that are metastable, as the well-known Graphite – Diamond transformation.

To date, ABO_3 perovskites are probably one of the most studied materials using HP-HT techniques. For instance, $MgSiO_3$ in the perovskite structure is the most abundant mineral on Earth and its HP-HT transformation explains the origin of the D'' seismic discontinuity in the deep lower mantle of the Earth[4]. HP-HT offers the possibility to incorporate cations that would never enter into the structure at ambient conditions, e.g. Mn^{2+} on the A-site of perovskites[5]. HP-HT has also allowed to isolate a homologous series of superconductors in which the number of CuO_2 planes incorporated increase with pressure[6]. Of course, this implies strong modifications in the resulting properties through the increase of the number of charge carriers in the structure. Another advantage is the possibility to modify the magnetic orderings[7] or electronic properties[8] through an amplification of the metallic behavior. All these aspects are summarized in a recent paper by Wang and Liu fully dedicated to the interest in using high-pressure experiments[9].

Krivovichev *et al*. published a paper dedicated to the use of HP-HT synthesis over anion-centered materials[10]. This is a class of materials described using building units centered on anions (here O^{2-}) and surrounded by cations (here Ln^{3+}) first evidenced by O'Keeffe and Hyde. [11,12] To date, the influence of HP-HT conditions over them has barely been studied. [13] In the case of Ln-based oxo-centered materials, it was mainly used for direct synthesis of rare-earth fluoride borates.[13] The combination of halides and borates appear particularly sensitive to HP-HT effects as pressure seems to be crucial in the formation of several lead oxychloride borates.[14] These HP-HT synthesis mimic the natural environment conditions for minerals to be formed.[15, 17] To date, the number of oxo-centered phases synthesized and/or modified under pressure is rather limited. We recently succeed in obtaining a new HP-HT polytype of the oxo-centered $BiCu_2PO_6$, well known for its exotic magnetic properties (spin gaped, S= ½ ladders, frustrated chains).[16] In the new polytype, the $_\infty[BiCu_2O_2]^{3+}$ double oxo-centered ribbons are kept whereas their orientation is changed and thus modifying the magnetic properties.

In situ high pressure Raman spectroscopy was chosen to explore the pressure-induced phase transformation due to its sensitivity to structural transitions. The spectral changes (appearance or disappearance) of Raman modes with pressure gives information about structural modifications of materials and might help to get new structures as done by Grzechnik et *al*.[18]

[a] *Université de Lille, CNRS, Centrale Lille, Université d'Artois, Unité de Catalyse et Chimie du Solide, Lille, F-59000, France*
[b] *MALTA-Consolider Team and Departamento de Química Física, Universidad Complutense de Madrid, E-28040 Madrid, Spain*
[c] *Univ. Lille, CNRS, INRA, ENSCL, UMR 8207 - UMET - Unité Matériaux et Transformations, Lille, F-59000, France*
[†] marie.colmont@centralelille.fr
Electronic Supplementary Information (ESI) available: [details of any supplementary information available should be included here]. See DOI: 10.1039/x0xx00000x

In this paper, we investigate the role of HP-HT conditions in obtaining innovative rare-earth based oxo-centered materials in the Li-Ln-V-O system after selecting pertinent samples through and using *in situ* high pressure Raman study. From the chemical point of view, this system is particularly interesting because only few structures are referenced to date: $LiLa_5O_5(VO_4)_2$[19], $LiLa_2VO_6$, a double perovskite[20] and $LaVO_4$ doped with several amounts of Li ions[21]. This kind of materials may generate high efficient luminescent properties either by doping with emitters [22,23] or by self-activation of vanadates.[24,25] Starting from the known $LiLa_5O_5(VO_4)_2$[19] phase, we have isolated by HP-HT synthesis two new inorganic phases: (**1**) *β*-$LiLa_5O_5(VO_4)_2$, (**2**) *β*-$LiLa_2O_2(VO_4)$ and obtained for the first time the related (**3**) $LiNd_5O_5(VO_4)_2$.

Experimental section

Synthesis

Stoichiometric amounts of Li_2CO_3, V_2O_5, $La(OH)_3$ or Nd_2O_3 have been mixed to various compositions as detailed in Table 1. The precursors have been preheated at 600 °C overnight in advance of weighing. The raw $LiLa_5O_5(VO_4)_2$ powder sample used as starting material was synthesized using the protocol detailed in ref. 19.

The original mixtures of **(1)** *β*-$LiLa_5O_5(VO_4)_2$, **(2)** *β*-$LiLa_2O_2(VO_4)$ and **(3)** $LiNd_5O_5(VO_4)_2$) were pre-reacted as powder samples. After grinding in an agate mortar, they were placed in an alumina crucible and heated at 600 °C for 12h. These mixtures were grinded and heated at 950 °C (**1**), 900 °C (**2**) or 1100 °C (**3**). All samples were cooled down to room temperature in this last step.

Raman spectroscopy

In situ high pressure Raman spectroscopy measurements were carried out between 1 and 15 GPa. Raman spectra were collected at room temperature on a backscattering confocal micro-Raman spectrometer (VoyageTM BWS435-532SY, BW&Tek) equipped with a CCD detector. The excitation was a 532 nm line from a solid-state laser, collected on the sample through an Olympus BX51 microscope with a 20x objective. Laser power was limited to 2 mW to avoid sample degradation. $LiLa_5O_5(VO_4)_2$ powder was loaded in a 100 µm diameter hole of a steel gasket in a Screw Driven Plate Diamond Anvil Cell (DAC) with diamond-culet sizes of 300 µm using silicone oil as hydrostatic pressure transmitting medium (PTM). In order to know the pressure inside the DAC, ruby spheres were placed next to the sample. The scheme of DAC organization is shown in figure S1 in Supplementary Information. The Raman spectra were registered in the 100-1500 cm^{-1} range of Raman-shift. At the end of the study, the sample cannot be recovered.

High Pressure - High temperature synthesis

Powders of each compounds were hard-packed in 5x2 mm^2 Platinum capsule and sealed. Reactions were done in a Piston Cylinder press equipped with a 1/2 inch cell. Series of experiments were performed at different pressure temperature conditions listed in Table 1. Throughout the experiment, the temperature was monitored with a W3Re–W25Re (Type D) thermocouple, the junction of which was placed near the sample. After the experiment, temperature was quenched and pressure was slowly released. The results are solid pellets made of a majority of powder assorted with tightly pressed small transparent crystals that were systematically studied.

XRD diffraction

Tiny single crystals of each new compound were selected and studied at room temperature using X8 4 circles diffractometer equipped with a 2D CCD 4K detector and an Ag micro-source for (**1**) and (**3**) and an APEX DUO diffractometer equipped with a 2D CCD 4K detector using a Mo-Kα source and an optical fiber acting as collimator for (**2**). JANA2006[26] program was used to solve the crystal structure using the Charge Flipping algorithm and then to refine it.

Powder X-ray diffraction data were collected at room temperature in the range of 2θ = 5 – 120°, with 0.02° step, 5 s counting time and using a D8 Advance Bruker AXS diffractometer in Bragg Brentano geometry equipped with a 1D LynxEye detector. Rietveld refinements were performed using TOPAS[27].

Table 1. Table of High Pressure - High temperature experiment conditions.

Stoichiometry			Target conditions		Result after powder X-Ray analysis
Li	La	V	P (GPa)	T(°C)/hr	
1	5	2	2	700/3	unreacted mixture
1	5	2	2	900/2	β-$LiLa_5O_5(VO_4)_2$, $La(OH)_3$, $LaVO_4$
1	5	2	2.5	900/12	β -$LiLa_5O_5(VO_4)_2$, $La(OH)_3$, $LaVO_4$
1	5	2	2	1000/2	β -$LiLa_5O_5(VO_4)_2$, $La(OH)_3$, $LaVO_4$
1	5	2	2	1050/3	β -$LiLa_5O_5(VO_4)_2$
1	5	2	2	1100/3	β -$LiLa_5O_5(VO_4)_2$
1	5	4	2	900/2	AP-$LiLa_5O_5(VO_4)_2$, $LaVO_4$
1	2	1	2	750/3	β -$LiLa_2O_2VO_4$, $La(OH)_3$, $LaVO_4$, $Li_{0.52}La_2O_{2.52}(CO_3)_{0.74}$
1	2	1	2	850/3	β -$LiLa_2O_2VO_4$, $La(OH)_3$, $LaVO_4$, $Li_{0.52}La_2O_{2.52}(CO_3)_{0.74}$
Li	**Nd**	**V**	**P (GPa)**	**T(°C)/hr**	**Result after powder X-Ray analysis**
1	5	2	2	1100/3	$LiNd_5O_5(VO_4)_2$

Magnetic measurements

Magnetic measurements were performed on a Physical Properties Measurement System (PPMS) Dynacool (9T) system from Quantum Design. Zero field cooling (ZFC) and field cooling (FC) procedures between 2 < T < 300 K under a 0.1 T magnetic field were measured.

Electron Microscopy

The high angle annular dark field (HAADF) image has been obtained on a TEM FEI TITAN Themis 300 equipped with a probe corrector giving a working resolution of 0.7 Å in STEM mode.

The powder was crushed and dropped in the form of alcohol suspension on carbon supported copper grids followed by evaporation under ambient condition.

Results and discussion

Evidence of phase transition by *in situ* high pressure Raman spectroscopy

In order to investigate $LiLa_5O_5(VO_4)_2$ sample, Raman spectroscopy was used since it is a very helpful tool for detecting small changes of the local symmetry in solids. Raman spectrum was registered for $LiLa_5O_5(VO_4)_2$ at ambient pressure in the Raman frequency shift of

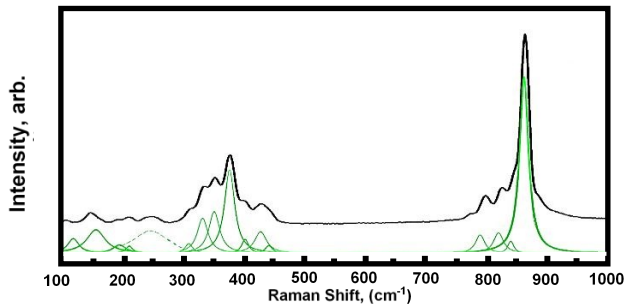

Figure 1: Room temperature-Ambient pressure Raman spectrum of $LiLa_5O_5(VO_4)_2$. Experimental data (in black line) are fitted with Lorentzian profiles (in green lines).

100-1500 cm^{-1}. Here we focused on the region 100-1000 cm^{-1} to avoid the signal of the diamond (Figure 1).

The number of Raman active modes were deduced using the Bilbao Crystallographic server. [28] $36A_g + 27B_g$ modes are expected and only 16 of them are measurable in our range of study, after Lorentzian deconvolution. The difference is supposed to be related to overlapping of Raman bands or to too small Raman scattering cross section. The spectra is rather complicated but at least the specific

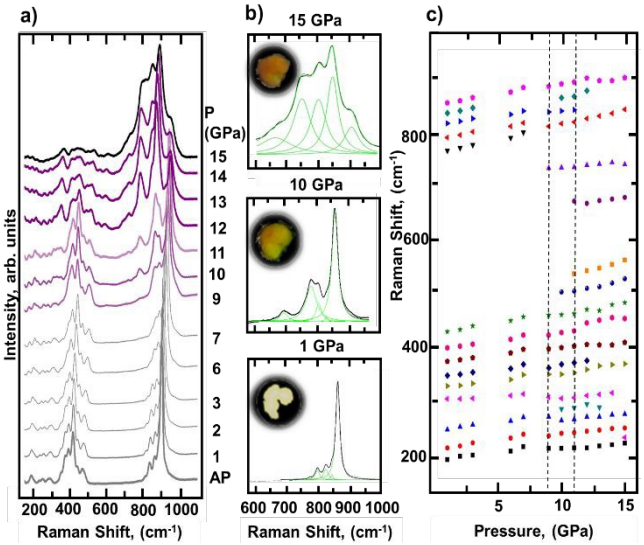

Figure 2: a) Evolution of Raman spectra from ambient pressure to 15 GPa (DAC) at room temperature, b) deconvolution of three spectra measured at 1, 10 and 15 GPa using Lorentzian profiles, insets show color changes with pressure and c) Pressure evolution of the identified Raman modes, dashed lines indicate average pressure of phase transitions.

Raman modes of vanadates are evidenced: up to 300cm^{-1}, rotational and translational modes; in the range 300-500 cm^{-1}, bending vibrations (O-V-O) and then above 700cm^{-1} the stretching modes (V-O) [29, 30, 31]. Also La/Li-O vibration modes are expected below 300 cm^{-1} [32].

Figure 2a shows the evolution of Raman spectra under pressure. Figure 2b shows the Lorentzian deconvoluted spectra at 1, 10 and 15 GPa on the spectral range 600-1000 cm^{-1}. The pressure evolution of Raman frequencies deduced from the deconvolution of each independent spectrum is shown in Figure 2c. First of all, an increase of the Raman frequencies for the 16 visible modes is observed upon higher pressure as expected as a consequence of bonds hardening and therefore the compression of the unit cell[33]. Secondly, changes occur around 9-10 GPa and 11-12 GPa. At 9-10 GPa new bands appear at 290, 510 and 745 cm^{-1} whereas the one at 811 cm^{-1} disappeared. Around 11-12 GPa, three modes disappear at 290, 380 and 854 cm^{-1}. These modifications can be explained by the structural changes occurring in the material. Another evidence of these possible phase transitions arises from color changes observed upon pressure using an optical microscope. The sample, initially white became successively yellow-green at 9 GPa and orange at 11 GPa (see Figure 2). *In situ* XRD will be needed in order to completely understand these spectral changes and directly correlate them with the structure but it was impossible in our working conditions. As a consequence, we used a combination of pressure and temperature in order to confirm structural changes *ex situ*. It is well known that temperature can help to reduce the pressure necessary to tackle the phase transition. For example, concerning the case of Mn_3TeO_6-I, a structural transition was evidenced around 18 GPa doing an *in situ* Raman spectroscopy in a diamond anvil cell without the use of high temperature[34]. At the same time, the new Mn_3TeO_6-II was isolated after modification of Mn_3TeO_6-I at 1173 K and 8 GPa, reducing the transformation pressure in 10 GPa by adding high temperature[35]. Following this idea, the achievement of the new structural types of $LiLa_5O_5(VO_4)_2$ was pursued using a Piston Cylinder Press able to work up to 3 GPa and 2000 K.

A first series of trials were started from Li:La:V stoichiometric ratio of 1:5:2. The precursors were weighed together and preheated at 600 °C prior to use. Working at 2 GPa and 700 °C, the sample did not react. By increasing the temperature to 900 °C, an unknown compound further assigned to phase (**1**) was observed. The purification of the sample was tested through two different ways: increasing pressure or temperature. The increase of pressure up to 2.5 GPa (while keeping temperature at 900 °C) led to obtain the targeted phase along with lanthanum hydroxide, which origin may come from absorbed water when loading the high pressure cell. A pure sample was achieved in the 1000 °C < T < 1100 °C temperature range, and tiny crystals were isolated and analyzed.

The new HP form of $LiLa_5O_5(VO_4)_2$

Tiny unshaped and colorless crystals of β-$LiLa_5O_5(VO_4)_2$ (**1**) were isolated and studied at ambient pressure using single crystal X-ray diffraction under conditions given in Table S1. (**1**) crystallizes in a triclinic unit cell with lattice parameters of a = 5.8167(15) Å, b =12.2954(28) Å, c =18.7221(69) Å, α =102.03(2)°, β = 98.76(2)°,

View Article Online DOI: 10.1039/D0DT02714J

γ = 103.54(2)° (S.G. *P*-1). The structure was solved using the charge flipping method[36] and refined with JANA2006[26]. There are 10 symmetrically independent lanthanum and 4 independent vanadium positions whose atomic and anisotropic thermal parameters were refined. 26 oxygen positions were added with isotropic thermal parameters.

A careful analysis of the Fourier difference maps evidenced residual electronic density in the empty spaces around the [VO_4] units. It was assigned to two lithium positions. Due to its light contribution close to heavier atoms, atomic positions and thermal parameters of lithium were fixed. At the end of the refinement, the reliability factor is R_F= 0.0759 and wR_F = 0.1031. The atomic positions and displacement parameters are listed in Supplementary Information Tables S2, and S3. The main interesting distances are gathered in SI Table S4 and bond valence calculations in Table S5. Structural data for β-$LiLa_5O_5(VO_4)_2$ phase were deposited with the number CSD-2005677.

it is commonly observed in related oxo-centered phases[19] ranging from 2.20(1) to 2.57(1) Å. There are two (for Li2) and one (for Li1) Li^+ cations per tunnel, along a period of about 5.8 Å (Figure 3d). The filling of square channels shows strong similarities with the AP phase (Figure 4a). In AP and HP crystal structures, one oxygen per [VO_4] group is involved in OLa_3 triangular units (*Tr*) which strengthen the polycationic backbone. A possible transformation process from the AP phase can be envisaged by the collapse of one of the step or height that completes the square channels in the HP form as presented in Figure 4b.

The [100] HAADF image for β-$LiLa_5O_5(VO_4)_2$ is shown in Figure 5a. Generally speaking, in the HAADF-STEM images, the contrast is proportional to the square of the atomic number (Z), which allows to consider these images as a projection of the structure with the heavy atoms brighter than the light ones. As observed from the crystal structure, the image confirmed the stacking by showing the perfect arrangement of the square

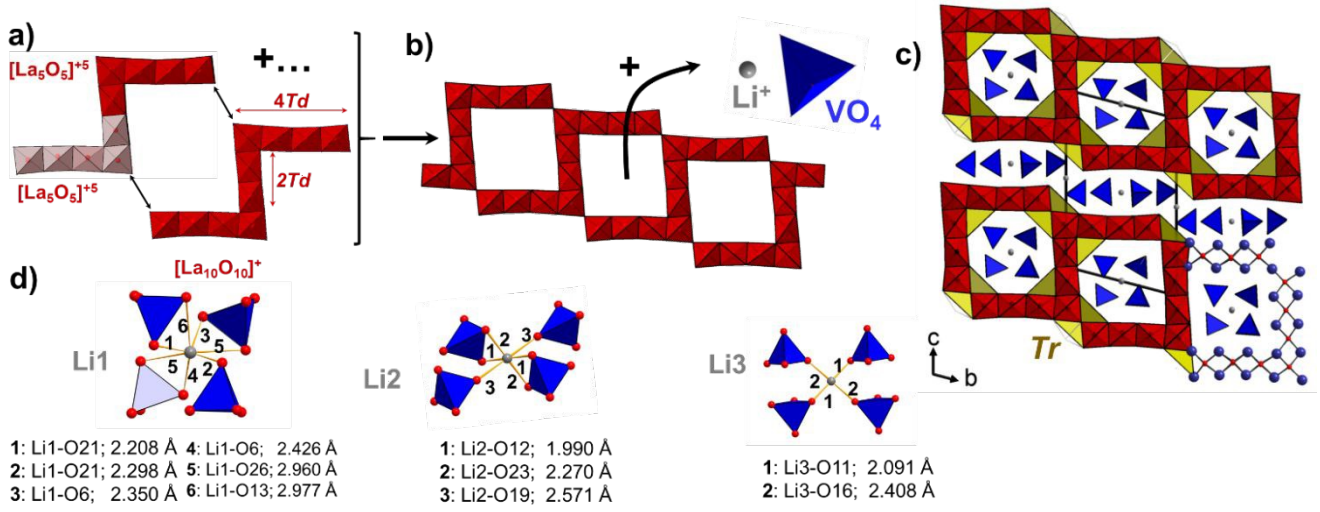

Figure 3: (a) Two $[La_5O_5]^{5+}$ units are connected together by edge sharing to build $[La_{10}O_{10}]^{10+}$ entity (b) sharing two corners with another $[La_{10}O_{10}]^{10+}$ unit leading to (c) 2D opened layers hosting VO_4 and Li^+ cations to build the HP form of $LiLa_5O_5(VO_4)_2$. The oxo-centered tetrahedra (Td) are marked by red and triangles (Tr) by yellow. (d) Geometrical environment of the Li sites in the structure of HP form of $LiLa_5O_5(VO_4)_2$

Another multi-dimensional open framework. The crystal structure of (**1**) is shown in Figure 3. The description is performed using the antiphase approach as it was the case for the AP (ambient pressure) polymorph[19]. The [OLa_4] tetrahedra (*Td*) show O-La bond length varying from 2.29(1) to 2.51(1) Å, in good agreement with what is classically observed for similar structures[37]. Five *T*d share common edges and form $[La_5O_5]^{5+}$ units of four 4 *Td* width and 2 *Td* height (Figure 3a). Two of these units are connected together by edge sharing of *T*d in the height, leading to another $[La_{10}O_{10}]^{10+}$ entity (Figure 3b). These entities are sharing corners to build 2D corrugated layers with 1D tunnels of 3*Td* width and height (Figure 3c). These tunnels are hosting four isolated vanadate.

The layers are stacked together, separated by sheets of isolated vanadate (Figure 3c). The association of [VO_4] marked out square channels and open spaces in layers and tunnels occupied by Li^+ cations respectively coordinated by four and six oxygen. Li-O bond distances are in the same order of magnitude as what tunnels and the layers. The white and the grey dots correspond to lanthanum and vanadium respectively, Li atoms are not visible. In some areas pointed out by red arrows in Figure 5a and c, some defects are evidenced. They are due to the substitution of vanadium by lanthanum inside the square tunnels so that it is possible to expect a substitution of [VO_4] groups by [OLa_4] *T*d.

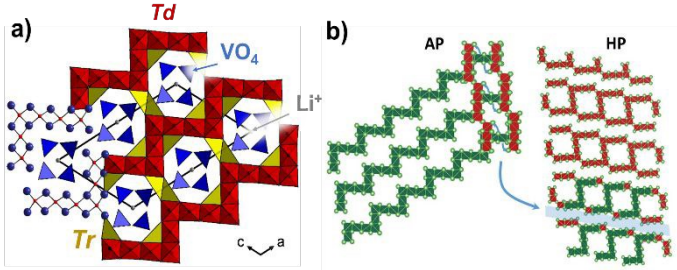

Figure 4: (a) crystal structure of AP-$LiLa_5O_5(VO_4)_2$ and (b) relationship between the AP and the HP form of $LiLa_5O_5(VO_4)_2$

A hypothetical representation of the structure of the defect is drawn on Figure 5c.

The presence of square channels was already observed in an oxo-centered phase but only based on Bi: $[Bi_{12}O_{15}]Li_2(SO_4)_4$[38] (structure shown in Figure S2) which is an example of a 3D porous network built on $[OBi_4]$ entities and hosting 1D channels with sulfates and Li^+ cations. There are also similar triangular $[OBi_3]$ units holding the polycationic network. To date in the literature, the multi-dimensional behavior (i.e. 2D layers with 1D tunnels) based on the association of oxo-centered units is scarce and only based on Bi-phases. Three examples have been reported so far, showing layers of triangular pores with various sizes of sections separated by sheets of chlorine[39]. To the best of our knowledge, this multi-dimensionality behavior is observed for the first time in Ln-based compounds. Here the application of pressure compress the structural units leading to the formation of unusual entities.

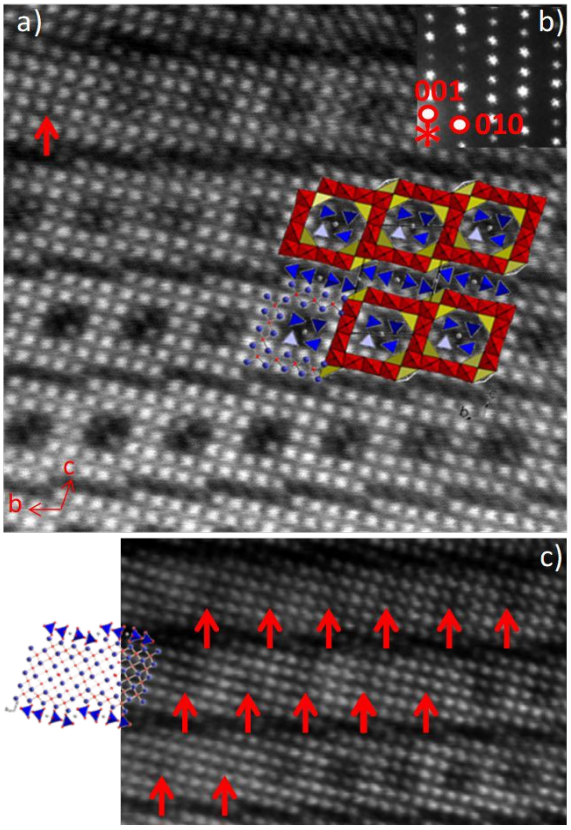

Figure 5: (a)[100] HAADF image and superimposition of the projected structure of the new -LiLa$_5$O$_5$(VO$_4$)$_2$. It clearly evidenced the [La$_5$O$_5$]$^{5+}$ layers (white dots corresponding to La atoms) and the darker part corresponding to the related [Li$_{0.5}$(VO$_4$)]$^{1.5-}$ tunnels and [Li$_{0.5}$(VO$_4$)]$_1^{5-}$ interlayer. (b) shows the corresponding indexed electron diffraction pattern (EDP) and (c) red arrows highlight areas where the square tunnels disappeared due to the local substitution of V by La atoms. The corresponding projected model is presented.

As already detailed in Table 1, the pure polycrystalline powder sample of HP-LiLa$_5$O$_5$(VO$_4$)$_2$ was successfully prepared using stoichiometric amounts of all elements and working at 2 GPa and 1000°C for 2 hours. The sample is pure as observed by powder XRD (see Figure S3) and the unit cell parameters were refined to a = 5.8295(2) Å, b = 12.3033(4) Å, c = 18.7438(5) Å, α = 102.115(1)°, β = 98.707(2)° and γ = 103.451(2)° in good agreement with the single crystal structure refinement.

In order to modify the magnetic or optical properties (*e.g.* as possible matrix hosting emitters for applications in WLEDS or lasers[40]) we tried to obtain the pure equivalent LiNd$_5$O$_5$(VO$_4$)$_2$ compound. The experiments using common synthesis conditions without pressure systematically failed. However, the use of HP-HT synthesis allowed us to obtain the desired composition as described in the following part.

Stabilization of LiNd$_5$O$_5$(VO$_4$)$_2$

The mixture of initial precursors was used in a 1:5:2 stoichiometric ratio of Li:Nd:V. Again, it was preheated at 600°C and used for HP-HT experiment following the same route as for (**1**). The pure sample was obtained at experimental conditions mentioned in Table 1. In this sample, tiny crystals were isolated and studied.

The single crystal structure of LiNd$_5$O$_5$(VO$_4$)$_2$ (**3**) was solved in the monoclinic space group $C2/m$ with cell parameters of a = 19.4507(2) Å, b = 5.7848(5) Å, c = 12.2593(1) Å and β = 117.847(5)° with Z = 2 (Table S11). LiNd$_5$O$_5$(VO$_4$)$_2$ is isostructural to the known AP-LiLa$_5$O$_5$(VO$_4$)$_2$ [19] which projection is shown in Figure 4a). The refinement satisfactory converged with residual factors refined to R_F = 0.0380 and wR_F= 0.0814. All main information are gathered in Tables S12, S13, S14 and S15. Structural data for phase **(3)** were deposited with the number CSD-2005696. The purity of the powder sample was confirmed by X-Ray diffraction (Figure S3). The unit cell parameters were refined to a = 19.4670(4) Å, b = 5.7881(1) Å, c = 12.2749(3) Å and β= 117.864(1)°, in good agreement with single crystal data. As expected, the rational use of high pressure allowed to synthesize the Nd phase isostructural with AP-LiLa$_5$O$_5$(VO$_4$)$_2$. The unit cell volume of (**3**) is smaller than the La analogue, in accordance with the lanthanide contraction as going through the series. As mentioned above, substitution of La for Nd opens up for further magnetic studies so the magnetic susceptibility for LiNd$_5$O$_5$(VO$_4$)$_2$ was measured. However, no transition was detected down to 2 K (Figure 6) probably due to the relative large distance between the Nd^{3+} cations (from 3.6 to 4Å). Curie-Weiss law fit gives C = 8.24 and θ = -34 K implying AFM

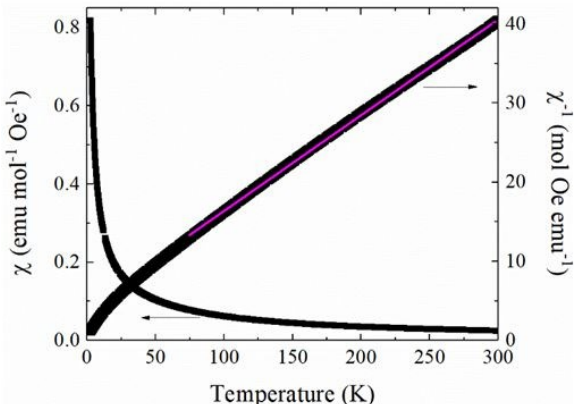

Figure 6. Direct and inverse magnetic susceptibility for LiNd$_5$O$_5$(VO$_4$)$_2$. The purple line shows a Curie-Weiss law fit.

interactions and an experimental value of μ_{eff} = 3.6 μ_B, in accordance with the theoretical value of μ_{theo} = 3.62 μ_B for Nd^{3+}. In order to investigate other possible compounds in this Li:La:V system, the initial 1:5:2 ratio has been switched to 1:2:1 and several trials done before obtaining the new $LiLa_2O_2VO_4$ (**2**) compound.

Crystal structure of (2) the new HP form of $LiLa_2O_2VO_4$

Mixture of precursors were grounded in an agate mortar and preheated at 600 °C before the HP-HT treatment. Tiny transparent colorless crystals of **(2)** have been obtained, isolated and measured. The crystal structure has been solved and refined using JANA2006 software[26].

The new β-$LiLa_2O_2VO_4$ crystallized in *P*-1 space group with *a* = 5.8144(7) Å, *b* = 5.8167(7) Å, *c* = 8.527(1)Å, α = 98.184(7)°, β = 100.662(7)° and γ = 92.579(7)° unit cell parameters (see Table S6). The procedure of solving and refining the structure exactly coincides with the one previously described for **(1)**. The structure presents 2 symmetrically independent sites for lanthanum. Both lithium and vanadium have just one unique symmetrically independent position. There are in total six oxygen positions. All atoms were well localized and refined with anisotropic thermal parameters. All information are gathered in Tables S7, S8 and S9. At the end of the refinement, residual factors led to R_F = 0.0494 and wR_F= 0.0564. Bond valence calculations for cations and anions are in good agreement with the expected values (see Table S10) and confirm the possibility to describe the structure in terms of oxo-centered tetrahedra. Structural data **(2)** were deposited with the number CSD-2005672.

[OLa_4] *Td* are formed around O(2) and O(3) atoms, with the O – La distances in a range of 2.345(5) to 2.466(3) Å. Oxo-centered *Td* shared common edges, forming $[La_2O_2]^{2+}$ infinite 2D layers. Between them, vanadium forms regular [VO_4] *Td*. Inside the vanadate, only O(1) atom is not shared with another tetrahedron. 2D infinite layers are formed by two [LiO_4] *Td* sharing an edge and all their oxygen being corner-shared with [VO_4] *Td* (see Figure 7d)). Li-O bond lengths are very regular varying from 1.959(6) to 1.974(9) Å (see Figure 7b). Different arrangements of [LiO_4] and [VO_4] polyhedrons exist and result in networks of variable dimensionality, for instance, 1D infinite chains in $LiMnVO_4$[42]. There, [LiO_4] and [VO_4] are edge-sharing and these two-component units form corner-sharing 1D chains. Rb_2LiVO_4 shows 2D layers based on edge- and corner-sharing [LiO_4] and [VO_4] tetrahedral.[43] 3D framework with tunnels are formed with corner-sharing [LiO_4] and [VO_4] as observed in $Ba_3Li_2V_2O_7Cl_4$.[44] To the best of our knowledge, $LiLa_2O_2VO_4$ sub-anionic layer appears to be innovative.

The crystal structure of β-$LiLa_2O_2VO_4$ is based on $[La_2O_2]^{2+}$ and $[LiVO_4]^{2-}$ layers. $[La_2O_2]^{2+}$ layers can be found in $La_2O_2(XO_4)$, (*X*= S, Mo or Cr) [45] (Figure 7 c and d). These $[Ln_2O_2]^{2+}$ anti-fluorite-type layers can be also observed in d-metal pnictide oxides.[46] The number of crystal structures found with these layers remain limited compared with those found with the equivalent $[Bi_2O_2]^{2+}$, mainly concerning Aurivillius phases. This is probably due to the bismuth capacity to fit into a more distorted tetrahedra due to its lone pair.

The X-ray powder diffraction analysis shows that the sample mainly corresponds to the new β-$LiLa_2O_2VO_4$ phase, with some impurities as $LaVO_4$[47] and $Li_{0.52}La_2O_{2.52}(CO_3)_{0.74}$[48] (see Figure S3). The refined unit-cell parameters are *a* = 5.7565(3) Å, *b* = 5.8036(3) Å, *c* = 8.4846(3) Å, α = 98.304(4)°, β = 100.560(4)° and γ = 93.383(4)°, in good agreement with the single crystal refinement.

Conclusions

The reasons in using high pressure for stabilizing new inorganic materials are various and have been largely detailed previously[49,50]. Our study is an example of several of these reasons. In the case of $LiLa_5O_5(VO_4)_2$ the new high pressure polymorph appears thanks to the so called '*densification effect*' that enables the stabilization of a phase/polymorph that would never be obtained without pressure. It is strongly linked to the compression of the entailed chemical bonds. The compression effects can be assessed by calculating the ratio of the unit cell volume and the corresponding number of chemical units. For the respective AP and HP phases of $LiLa_5O_5(VO_4)_2$, a decrease of 31 $Å^3$ is calculated and confirms the densification of the material. The case of $LiLa_2O_2(VO_4)$, is also interesting. The new phase evidenced in this paper is a polymorphic form of La_2LiVO_6, which is a double perovskite[20] synthesized at 6 GPa and 900 °C. Once more, this proves the necessity to combine HP-HT to reach this composition.[51] Concerning $LiNd_5O_5(VO_4)_2$, the purpose of using high pressure is to introduce smaller lanthanides into an existing matrix. Some examples exists in literature, mainly focused on perovskites in which La was successfully replaced by Pr or Nd[52].

Summarizing, we have used in situ DAC-Raman spectroscopy to identify a potential system for high pressure synthesis, Li-Ln-V-O. Three new phases have been obtained via HP-HT combined conditions. All of them can be described with oxo-centered tetrahedral units. HP-$LiLa_5O_5(VO_4)_2$ shows a straight relation to its AP- polymorph through a collapse of one of its building units through the application of pressure. The multi-dimensional behavior was also observed through HAADF microscopy. A new $LiLa_2O_2(VO_4)$ phase has been obtained with novel 2D layers. New $LiNd_5O_4(VO_4)_2$ has been also obtained and demonstrates that the incorporation of smaller rare earth cations is promoted

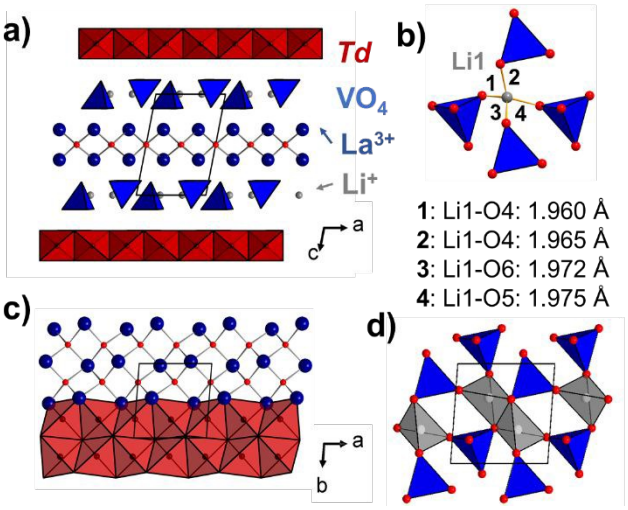

Figure 7: a) General projections of the β-$LiLa_2O_2VO_4$ crystal structure and b) Li atom tetrahedrally coordinated. Types of alternated layers: c) $[La_2O_2]^{2+}$ and d) $[LiVO_4]^{2-}$.

by high pressure. More extreme conditions may allow access the HP- polymorph for Ln = Nd. This work demonstrates the possibility to easily modify the original polymorphs, to access unknown structures and to incorporate other cations into oxo-centered based compounds through HP-HT treatments. This opens up a wide range of opportunities for the synthesis of new functional materials.

Acknowledgements

Chevreul Institute (FR 2638), Region Hauts-de-France, and FEDER are acknowledged for funding the X-ray diffractometers, HP-HT facilities and the PPMS magnetometer. The TEM facility in Lille (France) is supported by the Conseil Régional du Nord-Pas de Calais, and the European Regional Development Fund (ERDF). J.S-B. is grateful to the Ministerio de Ciencia, Innovacion y Universidades for the financial support under the project PGC2018-094814-B-C21. We also thank C. Minaud for helping with the magnetic measurements.

Conflicts of interest

There are no conflicts to declare.

Notes and references

1. J. B. Goodenough, J. A. Kafalas, *Phys. Rev.* 1967, **157**, 389;
2. J. B. Goodenough, J. A. Kafalas, J. M. Longo, P. Hagenmuller, Ed., *Academic*, 1972, 1-238;
3. C.-Q. Jin, J.-S. Zhou, J. B. Goodenough, Q. Q. Liu, J. G. Zhao, L. X. Yang, Y. Yu, R. C. Yu, T. Katsura, A. Shatskiy, E. Ito, *Proc. Natl. Acad. Sci. U.S.A* .2008, **105**, 7115–7119.
4. O. Tschauner, C. Ma, J. R. Beckett, C. Prescher, V. B. Prakapenka and G.R Rossman, *Science*, 2014, **346** *(6213)*, 1100-1102;
5. M. Markkula, A. M. Arevalo-Lopez, A. Kusmartseva, J. A. Rodgers, C. Ritter, H. Wu, *J.* Attfield, *Phys. Rev. B Condens. Matter*., 2011, **84**, 094450;
6. E. Takayama-Muromachi, *Chem. Mater.,* 1998, **10**, 2686-2698;
7. Á. M. Arévalo-López, E. Solana-Madruga, C. Aguilar-Maldonado, C. Ritter, O. Mentré, J. P. Attfield, *Chem. Commun*., 2019, **55**, 14470;
8. S.A. Khandy, I. Islam, Z.S. Ganai, D.C. Gupta, K.A. Parrey, *Journal of Elec Materi.,* 2018, **47**, 436–442;
9. X. Wang and X. Liu, *Inorg. Chem. Front*., 2020,
10. S. V. Krivovichev, O. Mentré, O. I. Siidra, M. Colmont, S. Filatov, *Chem. Rev.,* 2013, **113**, 6459−6535;
11. M. O'Keeffe, B. G. Hyde. *Structure and Bonding*, Springer, Berlin, Heidelberg, 1985, **61**, 77-144;
12. A. Navrotsky, M'O'Keeffe. *Structure and Bonding in Crystal,* Academic Press*,* 1981, **1**, 227, 299;
13. A. Grzechnik, P. F. McMillan, *J. Phys. Chem. Solids*, 1997, **58**, 1071–1078;
14. O. I. Siidra, H. Kabbour, O. Mentre, E. V. Nazarchuk, P. Kegler, D. O. Zinyakhina, M. Clmont, W. Depmeier, *Inorg. Chem*., 2016, **55**, 9077–9084;
15. S.M. Aksenov, V.S. Mironov, E.Y. Borovikova, N.A. Yamnova, O.A. Gurbanova, A.S. Volkov, O.V. Dimitrova, D.V. Deyneko, *Solid State Sci*., 2017, **63**, 16-22;
16. M. Colmont, C. Darie, A.A. Tsirlin, A. Jesche, C. Colin, O. Mentré, *Inorg. Chem.,* 2018, **57**, 6038-6044;
17. X. Yuan, C. Gao, J. Gao. 2019*, Mineral. Mag.*, **83***,* 191-197;
18. A. Grzechnik, P. F. McMillan, *J. Phys. Chem. Solids*. 1995, **56**, 159–164;
19. M. Colmont, L. Palatinus, M. Huvé, H. Kabbour, S. Saitzek, N. Djelal, P. Roussel, *Inorg. Chem*., 2016, **55**, 2252-2260;
20. J.-H. Choy, S.-H. Byeon, G. Demazeau. *J. Solid State Chem.,* 1988, **76**, 97-101;
21. S.W. Park, H. K. Yang, J. W. Chung, B. K. Moon, B. C. Choi and J. H. Jeong, *J. Korean Phy. Soc.,* 2010; **57**, 1764-1768;
22. R. Yu, J. H. Jeong, Y.-F. Wang, *J. Am. Ceram. Soc.,* 2017, **100**, 5649–5658;
23. A. M. Kaczmarek, D. Ndagsi, R. Van Deun, *Dalton Trans.,* 2016, **45**, 16231–16239;
24. P. Dang, D. Liu, Y. Wei, G. Li, H. Lian, M. Shang, J. Lin, *Inorg. Chem.,* 2020, **59**, 6026-6038;
25. S. Zhang, P. Zhang, Y. Huang, H. J. Seo, *J. Lumin.,* 2018, **207**, 460-464;
26. V. Petricek, M. Dusek, L. Palatinus, *Z. Kristallogr.,* 2014, **229**, 345-352;
27. A. A. Coelho, *J. Appl. Cryst.,* 2018, **51**, 210–218;
28. E. Kroumova, M. I. Aroyo, J. M. Perez-Mato, A. Kirov, C. Capillas, S. Ivantchev, H. Wondratschek, *Phase Transit.,* 2003*,* **76,** 155-170;
29. K. Cheng, C. Li, C. Yin, Y. Tang, Y. Sun, L. Fang. *J. Eur. Ceram. Soc.,* 2019, **39**, 3738-3743;
30. M. Azdouz, B. Manoun, M.Azrour, L. Bih, L. El Ammari, S. Benmokhtar, P. Lazor,, *J. Mol. Struct.,* 2010*,* **963**, 258-266;
31. M. Azdouz, B. Manoun, R. Essehli, M. Azrour, L. Bih, S. Benmokhtar, A. Aït Hou, P. Lazor., *J. Alloy. Compd.,* 2010, **498**, 42-51;
32. X. Cheng, D. Guo, S. Feng, K. Yang, Y. Wang, Y. Ren, Y. Song., *Opt. Mater.,* 2015, **49**, 32-38;
33. B. S. Araújo, A. M. Arévalo-López, C. C. Santos, J. P. Attfield, C. W. A. Paschoal; A. P. Ayala, *J. Appl. Phys*., 2020, **127**, 114102;
34. L. Liu, H. Skogby, S. Ivanov, M. Weil, R. Mathieu, P. Lazor, *Appl. Phys. Lett.,* 2019, **114**, 162903;
35. Á. M. Arévalo-López, E. Solana-Madruga, C. Aguilar-Maldonado, C. Ritter, O. Mentré, J. P. Attfield, *Chem. Commun.,* 2019, **55**, 14470;
36. L. Palatinus, G. Chapuis, *J. Appl. Crystallogr*., 2007, **40**, 786− 790;
37. M.A. Gomez Torres, G.H. Gauthier, A.M. Kaczmarek, M. Huvé, P. Roussel, V. Dupray, L. Yuan, A. Zadoya, M. Colmont, *Inorg. Chem.,* 2020, **59**, 5929-5938;
38. M. Lü, M. Colmont, M.Huvé, I. De Waele, C. Terryn, A. Aliev, O. Mentré, *Inorg. Chem.,* 2014, **53**, 12058-12065;
39. M. Lü, A. Aliev, J. Olchowka, M. Colmont, M. Huvé, C. Wickleder, O. Mentré, *Inorg. Chem.,* 2014, **53**, 528−536;

View Article Online
DOI: 10.1039/D0DT02721A

40. M. A. Al-Maliky, M. Frentzen, J. Meister, *Laser Med. Sci.,* 2019, **35**, 13-30;

41. S. V. Krivovichev, S. K. Filatov, *St. Petersburg University Press*: St. Petersburg, Russia, 2001;

42. A. K. Padhi, W. B. Archibald, K. S. Nanjundaswamy, J. B. Godenough, J. *Solid State Chem.,* 1997, **128,** 267–272;

43. R. Hoppe, J. Kissel, *Z. anorg. allg. Chem*., 1989, **571**, 113-126;

44. T. Reeswinkel, K. M. Sparta, G. Roth, *Acta Cryst*., 2008, **C64**, i38-i40;

45. D.O. Charkin, R.O. Grischenko, A.A. Sadybekov, R.J. Goff, P. Lightfoot, *Inorg. Chem.,* 2008, **47**, 3065–3071;

46. T. C. Ozawa, S. M. Kauzlarich, *Sci. Technol. Adv. Mater*., 2008, **9**, 033003;

47. C.E. Rice, W.R. Robinson, *Acta Cryst*., 1976, **B32**, 2232;

48. J. P. Attfield, G. Férey, *J. Solid State Chem.,* 1989*,* **82***,* 132–138*;*

49. G. Demazeau, H. Huppertz, J. A. Alonso, R. Pöttgen, E. Moran, J. P. Attfield, *Z. Naturforsch*., 2006, **61b**, 1457 – 1470;

50. G. Demazeau, *Z. Naturforsch.,* 2006, **61**, 799-807;

51. G. Demazeau, E. Oh-Kim, J. Choy, P. Hagenmuller, *Mat. Research. Bull.,* 1987, **22**, 735-740 ;

52. E. Solana-Madruga, Á. M. Arévalo-López, A. J. Dos Santos-García, E. Urones-Garrote, D. Ávila-Brande, R. Sáez-Puche, J. P. Attfield, *Angew. Chem. Int. Ed.,* 2016, **55**, 1 – 6;

Table of Content

View Article Online
DOI: 10.1039/D0DT02721A

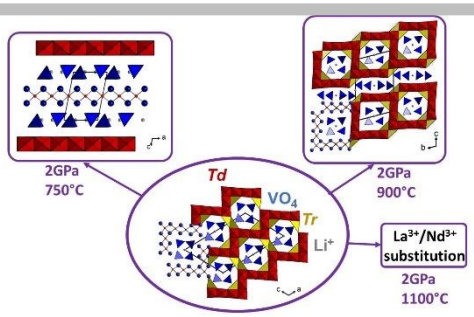

Zadoya, A. I.; Arévalo-López, Á. M.; Sánchez-Benítez, J.; Huvé, M.; Blach, J.-F.; Merkel, S.; Hilairet, N.; Chantel, J.; Colmont, M.

High pressure exploration in the Li – Ln – V – O system.

An in-situ high pressure Raman spectroscopy study on AP-$LiLa_5O_5(VO_4)_2$ allowed to evidence two new phases further stabilized using HP-HT synthesis.